Dispersion and the dissipative characteristics of surface waves in the generalized S transform domain

Roohollah Askari, Robert J. Ferguson

ABSTRACT

Wave number, group velocity, phase velocity and frequency dependent attenuation characterize the propagation of surface waves in dispersive, attenuating media. Here, a mathematical model is developed based on the generalized S transform to simultaneously estimate these characteristic parameters of surface waves from a seismic record. We use a scaling factor in the generalized S transform to enable application of method in highly dispersive medium. We introduce a cost functions in the S domain to estimate an optimum value for the scaling factor. We also use the cost function to generalize the application of the method for noisy data, especially data with a low signal to noise ratio at low frequencies. In that case, experimentally we find that estimated wave number is perturbed. As a remedy, we estimate wave number perturbation by minimizing the cost function using Simulated Annealing. We present synthetic and real data to show the efficiency of the method for the estimation of the propagation parameters of highly dispersive and noisy media. We anticipate that, through inversion of the characteristic parameters of surface waves, near surface shear wave velocity will be obtainable.

INTRODUCTION

Accurate estimation of shear wave (S-wave) velocity for near surface material such as soil, rocks and pavement is very important for many engineering and environmental purposes, as shear wave velocity is one of the essential properties used in stiffness coefficient determination (Xia et al., 2002a). Though seismic refraction methods are widely used for shear wave velocity studies (Palmer, 1980), they fail to estimate S-velocity where geological structure is complex (Xia et al., 2002b) or where hidden layers (a layer whose velocity is less than its upper layer) are present (Sheriff and Geldart, 1986).

An alternative to refraction analysis is surface wave analysis. Surface wave analysis is a well-known procedure where phase and group velocity of dispersive surface waves are inverted to estimate shear wave velocity structure (e.g. Evison et al., 1959; Stokoe et al., 1988; Keilis-Borok, 1989; Lay and Wallace, 1995; Xia et al., 1999). The usefulness of surface waves lies in their interaction with elastic and density discontinuities in the subsurface. Velocity varies with wavelength where discontinuities have an order of magnitude relationship to wave length (Park et al., 1999). This variation, known as dispersion, is observable on seismic records as a change in the period of successive wave cycles with time (Kennett, 1983).

Shear wave velocity is estimated from the inversion of phase and group velocity. Therefore the analysis of dispersion data to link phase and group velocity to frequency is a crucial step. Some algorithms have been developed to address these issues in different transform domains such as FK transform (Yilmaz, 1987), $\omega - p$ transform (McMechan and Yedlin, 1981) the phase shift (Park et al., 1998) and the wavelet transform (Kulesh et

al., 2005; Holschneider et al., 2005; Kulesh et all, 2008) for phase velocity, and narrow band-pass filtering (Herrmann, 1973) and the wavelet transform (Kulesh et al., 2005; Holschneider et al., 2005) for group velocity.

In this study, the generalized S transform (Pinnegar and Mansinha, 2003a) is used to estimate wave propagation parameters (phase velocity, group velocity and the attenuation function) for a highly dispersive medium and noisy data. The advantage of the S transform (Stockwell et al., 1996) and its generalized versions (e.g. Mcfadden et al., 2002; Pinnegar and Mansinha, 2003a; Pinnegar and Mansinha, 2003b; Pinnegar and Mansinha, 2004) lies in the fact that they provide frequency-dependent resolution while maintaining a direct relationship with the Fourier spectrum. Using this property, wave number and phase velocity are obtained directly from the absolute phase value of the ridges of the S domain, and group velocity is also computed from the time difference of the ridges of the transform. Frequency-dependent attenuation is estimated by the absolute amplitudes of the ridges of the transform. Kulesh et al. (2005) and Holschneider et al. (2005) propose a method for the estimation of the characteristic parameters of moderately dispersive surface waves based on the wavelet transform. Using a scaling factor introduced in the generalized version, we significantly improve estimation of the characteristic parameters of surface waves for highly dispersive data. Experimentally we find that estimated wave number is perturbed for noisy data when signal to noise ratio is small at low frequencies. As a remedy, we estimate wave number perturbation by minimizing a cost function using Simulated Annealing.

THEORY

The S transform is a time-frequency spectral localization method that is similar to the short-time Fourier transform (Gabor, 1946). The Gaussian window in the S transform is a function whose width and height scale, respectively, inversely and directly with frequency. The S transform is given by Stockwell et al. (1996) as

$$S[h(\tau)](t,f) = \int_{-\infty}^{+\infty} h(\tau) \left[\frac{|f|}{\sqrt{2\pi}} e^{-\frac{f^2(\tau-t)^2}{2}} \right] e^{-j2\pi f\tau} d\tau. \qquad (1)$$

where as an operator S transforms h into a function of frequency f and time t. Time t controls the position of the Gaussian window on the output time axis. The scaling property of the Gaussian window is reminiscent of the scaling property of continuous wavelets (Mallat, 1999) because one wavelength of the frequency f is always equal to one standard deviation of the window (Stockwell et al., 1996). The S transform, however, is not a wavelet transform, because the oscillatory parts of the S transform "wavelet" (provided by the complex Fourier sinusoid) does not translate with the Gaussian window when t changes. As a result, the shapes of the real and imaginary parts of the S transform "wavelet" change as the Gaussian window translates in time. True wavelets do not have this property because their entire waveform translates in time with no change in shape (Pinnegar and Mansinha, 2003b). Phase measured by the S transform is the localized value of absolute phase with respect to the Fourier spectrum (Pinnegar and Mansinha, 2003a). Thus, the S transform is conceptually a combination of short-time Fourier analysis and wavelet analysis.

A more general version of the S transform allows arbitrary variation in the window. The generalized S transform is

$$S_g[h(\tau)](t,f,\boldsymbol{p}) = \int_{-\infty}^{+\infty} h(\tau)w(\tau - t,f,\boldsymbol{p})e^{-j2\pi f\tau}d\tau, \tag{2}$$

where the Gaussian window of the S transform is generalized into the modeling window w whose width and shape are now a function of parameter $\boldsymbol{p}$. A version of the generalized S transform that has particular usefulness in our analysis is defined using

$$w(\tau - t,f,\boldsymbol{p}) = \frac{|f|}{\sqrt{2\pi}\gamma}e^{-\frac{f^2(\tau-t)^2}{2\gamma^2}}, \tag{3}$$

where, compared with the Gaussian window in equation (1), a scaling factor γ is introduced (Pinnegar and Mansinha, 2003a). Using γ, the generalized S transform is written

$$S_g[h(\tau)](t,f,\gamma) = \int_{-\infty}^{+\infty} h(\tau)\frac{|f|}{\sqrt{2\pi}\gamma}e^{-\frac{f^2(\tau-t)^2}{2\gamma^2}}e^{-j2\pi f\tau}d\tau, \tag{4}$$

where the scaling factor γ controls time-frequency resolution by changing the number of oscillations within the window. Figure 1 shows the Gaussian window for the scaling factors $\gamma =1$, 0.25 and 4 at a frequency of 10HZ respectively. When γ is smaller than one, the Gaussian window is tightened in the time domain and the time resolution increases. In the other hand, for γ larger than one, the Gaussian window is expanded in the time domain and therefore the frequency resolution increases. Figure 2a shows a signal which consists of three Ricker wavelets with central frequencies of 50HZ at 0.25s, 150HZ at 0.50s and 250HZ at 0.75s respectively. Figures 2b, 2c and 2d show the generalized S transforms of the signal for $\gamma=1$, 0.25 and 4 respectively. Figure 2c presents a better time resolution whereas Figure 2d presents a better frequency resolution. This phenomenon, as explained earlier, is pertinent to time-frequency expansion of the Gaussian window which is controlled by the scaling factor γ. In anticipation of the use of wave propagation operators cast in the Fourier domain, equation (4) is written (Pinnegar and Mansinha, 2003a)

$$S_g[h(\tau)](t,f,\gamma) = \int_{-\infty}^{+\infty} H(\alpha + f)e^{-\frac{2\pi^2\gamma^2}{f^2}\alpha^2}e^{j2\pi\alpha t}d\alpha. \quad f \neq 0, \tag{5}$$

where α is a frequency variable and

$$H(f) = \int_{-\infty}^{+\infty} h(\tau)e^{-j2\pi f\tau}\,d\tau \tag{6}$$

is the Fourier transform of $h(\tau)$.

THE WAVE PROPAGATION OPERATOR

Assuming geometrical spreading correction has been applied on surface wave data, if $h_1(\tau)$ is the wavelet at station 1, the wavelet $h_2(\tau)$ recorded at station 2 can be expressed

$$H_2(f) = e^{-\lambda(f)d}e^{-j2\pi k(f)d}H_1(f), \tag{7}$$

where $\lambda(f)$ is an attenuation function, and $k(f)$ is a spatial wave number that controls wave propagation from station 1 to station 2. This wave number characterizes horizontal propagation of surface wave and is a function of elastic properties of the medium, and d is the distance between, the two stations. This relation is written in the S domain as

$$S_g[h_2(\tau)] = \int_{-\infty}^{+\infty} e^{-\lambda(f+\alpha)d}e^{-j2\pi k(f+\alpha)d}H_1(\alpha + f)e^{-\frac{2\pi^2\gamma^2}{f^2}\alpha^2}e^{j2\pi\alpha\tau}d\alpha. \tag{8}$$

Klush et al. (2005) assume that attenuation function $\lambda(f)$ and phase function $k(f)$ vary slowly with respect to the effective size of the spectrum of the wavelet transform. We make the same assumption for the generalized S transform. For instance, for fixed point (t, f) on the time-frequency plane, we may develop λ and k around the central frequency f. For moderate dispersion, the wave number term $k(f)$ on the right-hand side of equation (8) can be approximated by the first two terms of its Taylor series around f. So, $\lambda(f + \alpha)$ and $k(f + \alpha)$ can be expressed

$$\lambda(f + \alpha) = \lambda(f) + O(\alpha), \tag{9}$$

and

$$k(f + \alpha) = k(f) + \alpha k'(f) + O(\alpha^2), \tag{10}$$

where $k'(f)$ indicates a frequency derivative of $k(f)$. Upon inserting the above approximations into the integral (8), we obtain

$$S_g[h_2(\tau)](t, f, \gamma) = \int_{-\infty}^{+\infty} e^{-\lambda(f)d}e^{-j2\pi(k(f)+\alpha k\prime(f))d}H_1(\alpha + f)e^{-\frac{2\pi^2\gamma^2}{f^2}\alpha^2}e^{j2\pi\alpha\tau}d\alpha$$

$$= e^{-j2\pi k(f)d}e^{-\lambda(f)d}\int_{-\infty}^{+\infty} H_1(\alpha + f)e^{-\frac{2\pi^2\gamma^2}{f^2}\alpha^2}e^{j2\pi\alpha(\tau-k\prime(f)d)}d\alpha$$

$$= e^{-j2\pi k(f)d}e^{-\lambda(f)d}S_g[h_1](t - k'(f)d, f), \tag{11}$$

where $S_g[h_1](t - k'(f)d, f)$ is the generalized S transform of h₁ shifted by $-k'(f)d$. Considering

$$v_p(f) = f/k(f) \tag{12}$$

where v_p is phase velocity that is the velocity of each frequency component of surface wave, and also

$$v_g(f) = 1/k'(f), \tag{13}$$

where group velocity v_g is the velocity of a wave pocket (envelope) of surface wave around frequency f, equation (11) is expressed as

$$S_g[h_2(\tau)] = e^{-j2\pi f d/v_p(f)} e^{-\lambda(f)d} S_g[h_1(\tau)]\left(t - d/v_g(f), f\right). \tag{14}$$

Based on equation (14), any point at time-frequency plane (t, f) of station 1, is equivalent to the time shifted-frequency plane (t-$d/v_g(f)$, f) of station 2 whose phase difference is $-j2\pi f d/v_p(f)$, and whose amplitude is proportional to $e^{-\lambda(f)d}$ that of station 1. Thus, the group velocity can be obtained from the time difference of the ridge of the transforms for any frequency, and the phase velocity can be computed from their phase difference. Figure 3 is given to show how to use equation (14) in order to obtain the propagation parameters. Figures 3a and 3b show the amplitude spectra of the generalized S transform of two stations respectively. Figure 3c and Figure 3d show their phase spectra respectively. At the first step, ridges of the amplitude spectra of the transform are found (Figures 3a and 3b) at any specific frequency (here f =150HZ) with respect to the time axis. Attenuation is obtained as

$$\lambda(f) = \frac{[\log(A_1(f)/A_2(f))]}{d}, \tag{15}$$

where A_1 and A_2 are the absolute, maximum amplitudes of the ridges of the stations receptively. Group velocity is obtained as

$$v_g = \frac{d}{\Delta t}, \tag{16}$$

where $\Delta t = t_2 - t_1$(from Figures 3a and 3b) is the time difference between two ridges. Wave number $k(f)$ is computed

$$k(f) = \frac{\Delta\varphi}{2\pi d}, \tag{17}$$

where $\Delta\varphi$ is phase differences between two ridges (Figures 3c and 3d). Finally phase velocity is calculated using equation (12).

Comparing equation (14) with that proposed by Kulesh et al. (2005) for the wavelet transform, one observes that the phase velocity obtained from the generalized S transform is directly related to the phase spectrum because the phase in the generalized S transform is a localized value of the absolute phase with respect to the Fourier spectrum, whereas the phase in the wavelet transform is instant. Equation (14) takes advantage of calculating the phase velocity independently from the group velocity, so any error in calculating the group velocity does not impact on the estimation of phase velocity.

At first glance, the assumption applied in equations (11) and (12) might lead us to the conclusion that any propagation parameter estimation based on the generalized S transform would make sense only for wave propagation in weakly dispersive media at low frequencies where there is a linear phase process. In cases where the medium is highly dispersive, and a signal has a wide band of frequencies, there is more uncertainty to accurately estimate amplitude and phase spectra of high frequencies due to low frequency resolution which is indicated by Heisenberg boxes (Mallat, 1999). However, the generalized S transform improves frequency resolution of high frequencies by selecting a larger value of γ. So it provides a better estimation of amplitude and phase

spectra of high frequencies. Thus it is able to estimate propagation parameters of surface wave for highly dispersive and attenuating media.

Figure 4 shows a wavelet signal dispersed in a relatively high dispersive medium with a dominant frequency of 125 HZ. Geophone spacing is assumed to be 250 m. As seen in Figures 5a, 5b, 3c and, 5d wave number, group velocity and attenuation obtained using scaling factor γ=20 are poorly estimated for higher frequencies. This error implies the phase and amplitude spectra of high frequencies are poorly estimated. If a larger scaling factor is chosen, the Gaussian window expands in the time domain, and frequency resolution increases. So, we expect to improve results by choosing larger values for γ for this example. The dotted lines in Figure 5 show the estimated propagation operators based on γ=100. The wave number and phase velocity are now well estimated for all frequency components. The group velocity for lower frequencies (0-4 HZ) is not poorly estimated due to low time resolution for low frequencies. But for higher frequencies the result is acceptable. The estimated attenuation function is well computed for frequency ranges from zero to 220 HZ, and for frequency ranges from 220 HZ to 250 HZ, the attenuation function is underestimated. One approach to get a better estimation of the attenuation function is to select higher values of γ. When a higher value of γ is selected, the time resolution is weakened, so the possibility of the time-frequency overlap of higher modes increases. Thus, we are limited to choosing higher values of γ in practice. To compare amplitude and phase spectrum of signals based on different values of the scaling factor, the amplitude and phase spectrum of traces (1) and (7) for scaling factors γ=20 and γ=100 are shown in Figure 6. Figure 7 shows the predicted data based on the estimated wave number and attenuation function based on the scaling factor γ=100 for traces (2), (4) and (6) respectively (the dashed lines). The estimated wave number and attenuation function are able to predict data close to that of the reference model.

An optimum value for γ is obtained using a cost function

$$E(\gamma) = \left\| S_{g_i}(t,f) - S_{g_r}\left(t - D_i/v_g(f), f\right) e^{-\lambda_{\gamma(f)}D_i} e^{-i2\pi k_{\gamma(f)}D_i} \right\|^2, \qquad (18)$$

where $\lambda_\gamma(f)$ is the calculated attenuation and $k_\gamma(f)$ is the calculated wave number based on a specific value of γ respectively, S_{g_i} is the generalized S transform of the ith geophone, S_{g_r} is the generalized S transform of a reference geophone which could be the first geophone and D_i is the distance between the reference and i[th] geophones. Figure 8 shows the cost function for the data. As seen the cost function converts to zero for γ larger than 70. It implies we should choose γ larger than 70 to have good estimations of the attenuation and the wave number.

Figures 9a and 9b show two dispersed synthetic data sets with different dispersivities. In the both models, a Ricker wavelet is with a dominant frequency of 125 HZ is used as the seismic wavelet and geophone spacing is assumed to be 250 m. Figures 9c and 9d show phase velocities for Figures 9a and 9b respectively. Phase velocity for Figure 9a has velocity ranges from 760 m/s to 850 m/s whereas the velocity ranges for Figure 9b vary from 800 m/s to 1400 m/s. Therefore the second data set is more dispersed in comparison with the first data set. However it is less dispersed than the data used in Figure 1 where its phase velocity varies from 850 m/s to 1950 m/s. Figures 9e and 9f show the cost

function for the both data sets respectively. The cost function for the first data converts to zero at $\gamma = 5$ and for the second data converts to zero at $\gamma = 22$. It can be concluded for higher dispersive media, a higher value of γ should be chosen. In other words, γ is a function of the dispersivity of a medium.

EXAMPLES

Synthetic Data Example

To investigate noise effect on the estimation of propagation parameters using the generalized S transform, two synthetic seismic records are analyzed. In the first model (Figure 10), a Gaussian wavelet with standard deviation 7×10^{-3} is used. The additive noise is white Gaussian with a standard deviation of .01, and where the geophones are irregularly spaced. The average distance between two adjacent geophones, however, is set to be 200m. In the second model (Figure 11) a Ricker wavelet with dominant frequency 22.5 HZ is used. All other parameters are identical with that used in the first model. The theoretical propagation parameters correspond to the solid lines in Figure 12. The dashed lines in Figure 12 are the estimated parameters obtained from the first model. As may be seen in Figure 12, the wave number and the phase velocity are well estimated in comparison with the theoretical values. The group velocity and the attenuation function are relatively well estimated around low frequencies where the Gaussian wavelet has more energy (Figure 13). The estimated group velocity, however, seems distorted around zero frequency. As explained earlier, it can be referred to low time resolution at low frequencies. The dotted lines in Figure 12 are the estimated propagation parameters for model 2. The estimated wave number and phase velocity are not consistent with the theoretical values. The wave number of the model (k_m) can be expressed as approximately equal to the estimated wave number (k_e) plus perturbation according to

$$k_m \approx k_e + \varepsilon. \tag{19}$$

Equation (19) can be explained by the effect of noise at low frequency components where the signal to noise ratio is small because the Ricker wavelet has less energy at low frequencies (Figure 13). At those frequencies, initial values of phase (φ_0) are highly affected by noise, hence, any phase difference between two geophones is not directly proportional to the wave number. The group velocity and the attenuation function are better estimated around frequency 22.5 HZ where signal to noise ratio is high. The group velocity is more highly distorted around zero frequency due to the small amount of signal to noise ratio and also low time resolution at low frequencies. Based on the estimated parameters, the predicted traces for geophones (2), (9) and (15) for both models are computed. Figure 14 shows the predicted traces (the dashed lines) for the first model. The estimated wave number and attenuation function have been able to predict the model appropriately. Figure 15 shows the predicted traces (the dashed lines) for the second model. As seen, the envelopes for the predicted and the real traces seem to be the same, implying the group velocities are equal. This fact can be obtained by equation (19) too. However, they do not fit each other due to wrong estimation of the group velocity.

The problem can be solved using the least squares solution by finding an appropriate value for wave number perturbation ε. The assumption is $|\varepsilon| \ll 1$. The cost function is to be minimized.

$$E(\varepsilon) = \left\| S_{g_i}(t,f) - S_{g_r}\left(t - D_i/v_g(f), f\right) e^{-\lambda(f)D_i} e^{-i2\pi k_e(f)D_i} e^{-i2\pi\varepsilon D_i} \right\|^2, \quad (20)$$

where S_{g_i} is the generalized S transform of the ith geophone, S_{g_r} is the generalized S transform of a reference geophone which in this study the first geophone is assumed as the reference and D_i is the distance between the reference and i[th] geophones. Figure 16 show the error function for $0 < \varepsilon < .1$. The cost function is highly non-linear and has lots of local minima, so it is impossible to solve it using some gradient methods such as Steepest Descent or Conjugate Gradient. In this paper, Simulated Annealing (Beaty et al., 2002) is used to find an optimum value for epsilon. Each step of Simulated Annealing replaces the current solution by a random "nearby" solution, chosen with a probability that depends on the difference between the corresponding function values and on a global parameter (called the temperature), that gradually decreases during the process. For the second model, the optimum value of $\varepsilon = 0.00189414$ is obtained. Figure 17 shows the wave number and the phase velocity corrected based on the computed value for epsilon. The corrected wave number and corrected phase velocity match very well with that of the theoretical. Figure 18 show the predicted traces based on the corrected wave number. As seen, the predicted traces match better to the data.

The reason why the geophones are assumed to be irregularly spaced is that for distances larger than 100m, it is possible to find many values of small epsilons minimizing equation (20). For instance, if the distance between two adjacent geophones is 100m, "$\varepsilon + .01$" will give the same amount of error as epsilon because the multiplication of .01 by the distance will produce an integer multiple of 2π. In practice, in seismic exploration, geophone spacing is usually less than 100m, so it need not be irregularly spaced. In earthquake seismology the distance between two adjacent seismometers is much larger than 100m. Nevertheless, seismometers are usually irregularly spaced; hence, we can use the least squares solution to find an optimum value of epsilon for noisy data in the both seismic and seismological studies.

Real Data

Figure 19 (solid lines) shows a real seismic record consisting of dispersive surface wave with sampling frequency 1000 HZ and sampling distance one meter. Figure 20 shows the estimated propagation parameters obtained from the generalized S transform. Based on the estimated wave number and attenuation function other traces are predicted. The dashed lines in Figure 19 show the predicted traces from the first trace (the first geophone). The predicted traces are well matched to the real data implying good estimation of the wave number and attenuation function.

CONCLUSIONS AND DISCUSSIONS

In this study we use a mathematical model to link the time-frequency spectrum of a signal based on the generalized S transform to its propagation parameters (wave number, phase velocity, group velocity and attenuation function) in dispersive and attenuating

media. The S transform and its generalized versions provide frequency-dependent resolution while maintaining a direct relationship with the Fourier spectrum. Using this property, wave number and phase velocity are obtained directly from the absolute phase value of the ridges of the S domain. Group velocity is also computed from the time difference of the ridges of the transform. Finally, frequency-dependent attenuation is estimated by the absolute amplitudes of the ridges of the transform. The advantage of the generalized S transform over the S transform lies in the fact that it manipulates time-frequency resolution in the S domain using a scaling factor. Therefore results can be improved, especially for a highly dispersive and dissipative medium. According to the results of the synthetic data, for a highly dispersive medium, a larger value of the scaling factor must be chosen. In general, estimated parameters are more reliable where signal to noise ratio is high. However, group velocity estimated for frequency ranges (0-5) HZ is not satisfactory due to low time resolution of the transform at low frequencies. This limits the ability of the method to determine the group velocity at mentioned frequency ranges.

In reality, a seismic signal usually consists of several modes of surface waves. If time-frequency spectrum of different modes of the signal in the S domain is well separated, it is quite possible to simultaneously extract the propagation factors of different modes with respects to their time-frequency distributions. However, we are usually limited to choosing an appropriate scaling factor due to overlapping time-frequency spectrum of different modes for specific values of the scaling factor. We introduce a cost function to estimate a minimum optimum value for the scaling factor. We could make decision what ranges of the scaling factor should be chosen based on the minimum value of the scaling factor and also overlapping time-frequency spectrum of different modes.

Experimentally we find that estimated wave number is perturbed for noisy data when signal to noise ratio is small at low frequencies. As a remedy, we estimate wave number perturbation by minimizing a cost function using Simulated Annealing. As discussed earlier, for receiver spacing larger than 100m, receivers must be irregularly deployed to have a unique answer for the cost function.

ACKNOWLEDGEMENTS

REFERENCES

Beaty, K. D.R. Schmitt, and M. Sacchi, 2002, Simulated annealing inversion of multimode Rayleigh wave dispersion curves for geological structure: Geophys. J. Int., 151, 622-671

Evison, F. F., Orr, R. H., and, Ingham, C. E., 1959, Thickness of the earth's crust in Antarctica: Nature, 183, 306-308.

Gabor, D., 1946, Theory of communication: J. Inst. Elect. Eng., 93, 429–457.

Herrmann, R. B., 1973, Some aspects of band-pass filtering of surfacewaves: Bull. seism. Soc. Am, 63, 663–671.

Holschneider, M., Diallo, M. S., Kulesh, M., Ohrnberger, M., Lück, E., and Scherbaum, F., 2005, Characterization of dispersive surface waves using continuous wavelet transforms: Geophys. J. Int., 163, 463–478.

Keilis-Borok, V. I., 1989, Seismic Surface Waves in Laterally Inhomogeneous Earth: Kluwer Academic Publishers, London.

Kennett, B. L. N., 1983, Seismic Wave Propagation in Stratified Media: Cambridge University Press, Cambridge, UK.

Kulesh, M., Holschneider, M., Diallo, M. S., Xie, Q., and Scherbaum, F., 2005, Modeling of wave dispersion using continuous wavelet transforms: Pure and Applied Geophysics, 162, 843–855.

Kulesh, M., Holschneider, M., Ohrnberger, M., and Lück. E., 2008, Modeling of wave dispersion using continuous wavelet transforms II: wavelet-based frequency-velocity analysis: Pure and Applied Geophysics, 165, 255–270.

Lay, T., and Wallace, T. C., 1995, Modern Global Seismology: Academic Press, London, UK.

Mallat, S., 1999, A wavelet tour of signal processing: Academic Press, London, UK.

Mcfadden, P. D., Cook, J. G., and Forster, L. M., 2002, Decomposition of gear vibration signals by the generalized S transform: Mechanical Systems and Signal Processing, 13, 691-707.

McMechan, G., and Yedlin, J. M., 1981, Analysis of dispersive waves by wave field transformation: Geophysics, 46, 869-874.

Palmer, D., 1980, The generalized reciprocal method of seismic refraction interpretation: Society of Exploration Geophysicists, Tulsa, OK, 104 p.

Park, C. B., Miller, R. D. and Xia, J., 1998, Imaging dispersion curves of surface waves on multi-channel record, Technical Program with Biographies SEG, 68th Annual Meeting, New Orleans, LA., 1377–1380.

Park, C.B., and Miller, R.D., Xia, J., 1999, Multichannel analysis of surface waves: Geophysics, 64, 800–808.

Pinnegar, C. R., and Mansinha, L. 2003a, The Bi-Gaussian S-transform: SIAM J. SCI. COMPUT., 24, 1678–1692.

Pinnegar, C. R., and Mansinha, L., 2003b, The S-transform with windows of arbitrary and varying shape: Geophysics, 68, 381–385.

Pinnegar, C. R., and Mansinha, L., 2004, Time-local Fourier analysis with a scalable, phase-modulated analyzing function: the S-transform with a complex window: Signal Processing, 84, 1167 – 1176.

Sheriff, R.E., and Geldart, L.P., 1986, Exploration Seismology, Vol. 12. Cambridge University Press, Cambridge, UK.

Stockwell, R. G., Mansinha, L., and Lowe, R. P., 1996, Localization of the complex spectrum: The S transform: IEEE Transactions on Signal Processing, 44, 998-1001.

Stokoe II, K.H., Nazarian, S., Rix, G.J., Sanchez-Salinero, I., Sheu, J., and Mok, Y., 1988. In situ seismic testing of hard-to-sample soils by surface wave method: Earthquake Engineering and Soil Dynamic. II — Recent adv. in ground-motion eval. ASCE, Park City, pp. 264–277.

Xia, J., Miller, R.D., and Park, C.B., 1999, Estimation of near-surface shear-wave velocity by inversion of Rayleigh waves: Geophysics, 64, 691–700.

Xia, J., Miller, R. D., Park, C. B., Hunter, J. A., Harris, J. B., and Ivanov J, 2002a, Comparing shear wave velocity profiles inverted from multichannel surface wave with borehole measurements: Soil Dynamics and Earthquake Engineering, 22, 181-190.

Xia, J., Miller, R. D., Park, C. B., Wightman, E., and Nigbor, R., 2002b, A pitfall in shallow shear-wave refraction surveying: Journal of Applied Geophysics, 51, 1 – 9.

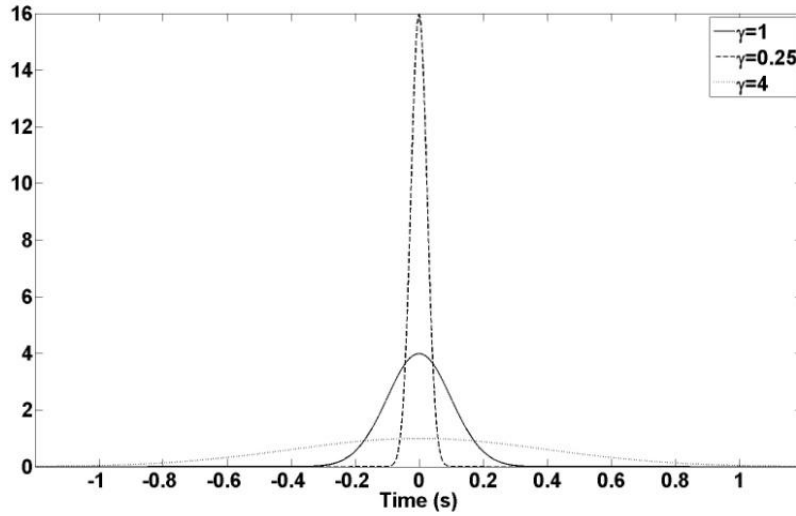Yilmaz, O., 1987, Seismic Data Processing: Soc. Exploration Geophysicists, Tulsa, OK.

FIG. 1. The Gaussian window at the frequency of 10HZ for γ=1 (the solid line), γ=0.25HZ (the dashed line) and γ=4 (the dotted line).
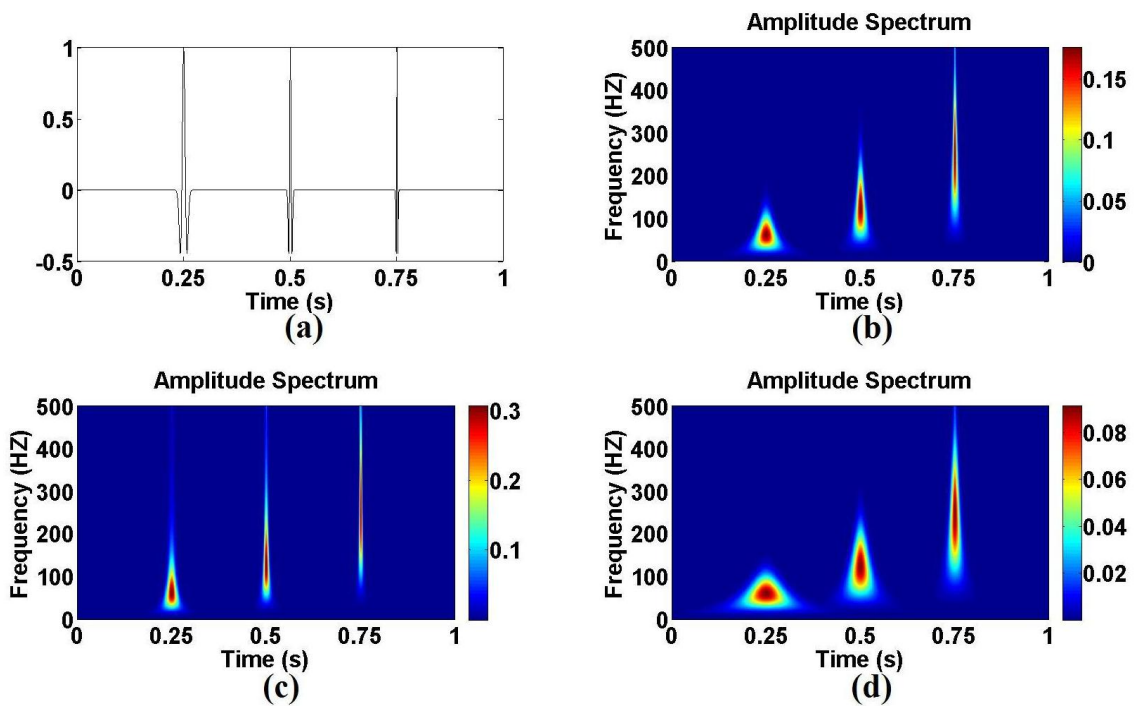

FIG. 2. (a) a signal. (b), (c) and (d) the generalized S transforms of (a) for γ=1, 0.25 and 4 respectively.
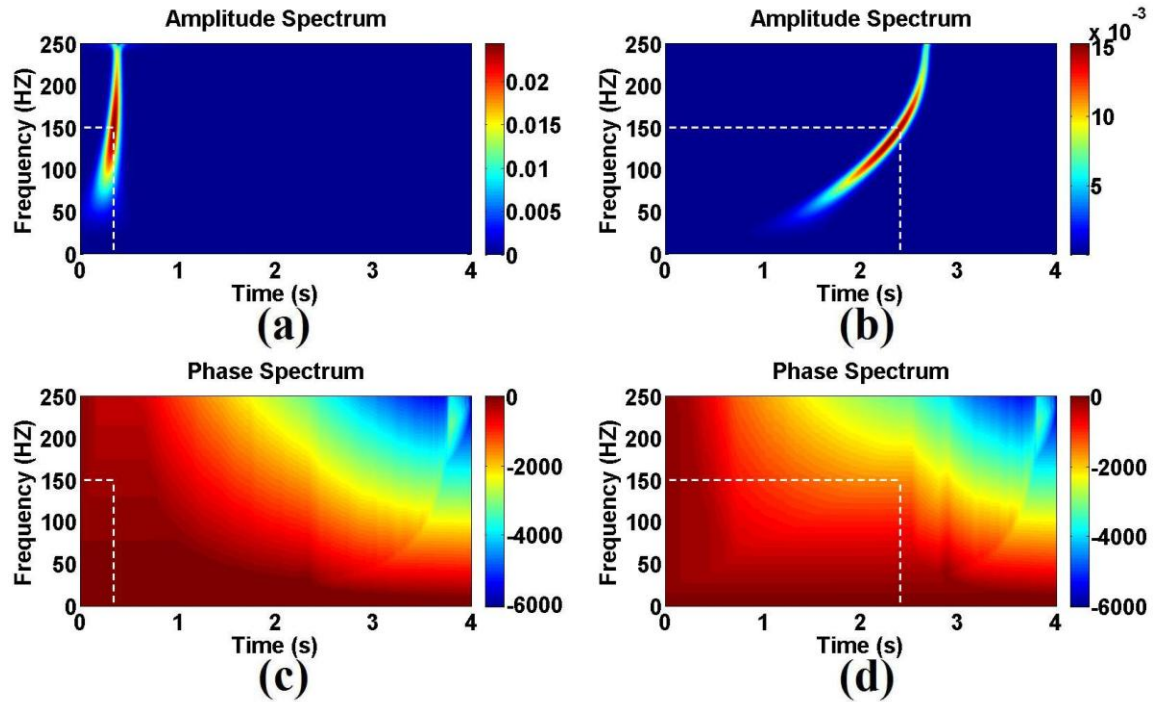
FIG. 3. (a) the amplitude spectra of the first station. (b) the amplitude spectra of the second station. (c) the phase spectra of the first station. And (d) the phase spectra of the second station. The dashed line show how time and phase information of the ridges is estimated.
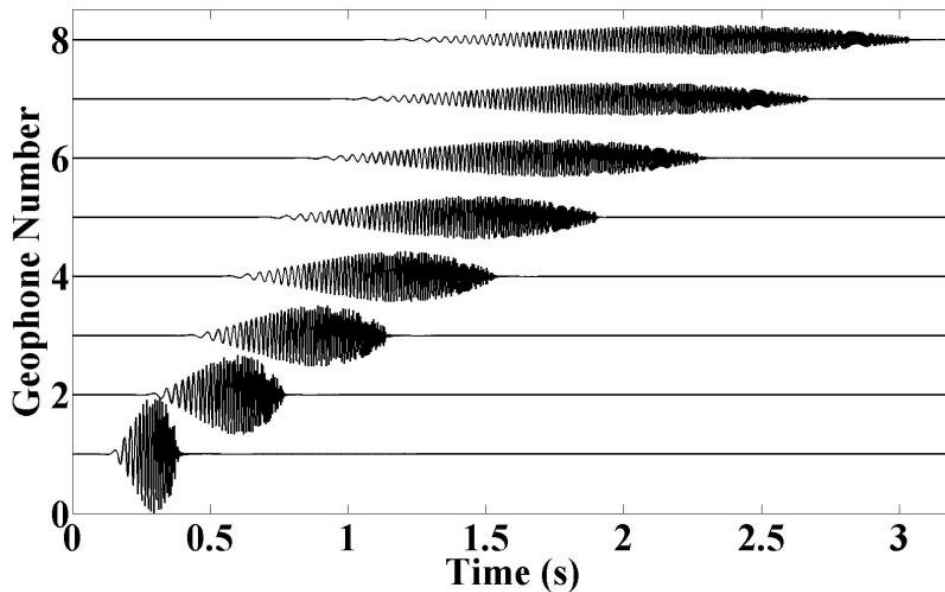
FIG. 4. A wavelet signal dispersed in a relatively high dispersive medium recorded at different geophones.
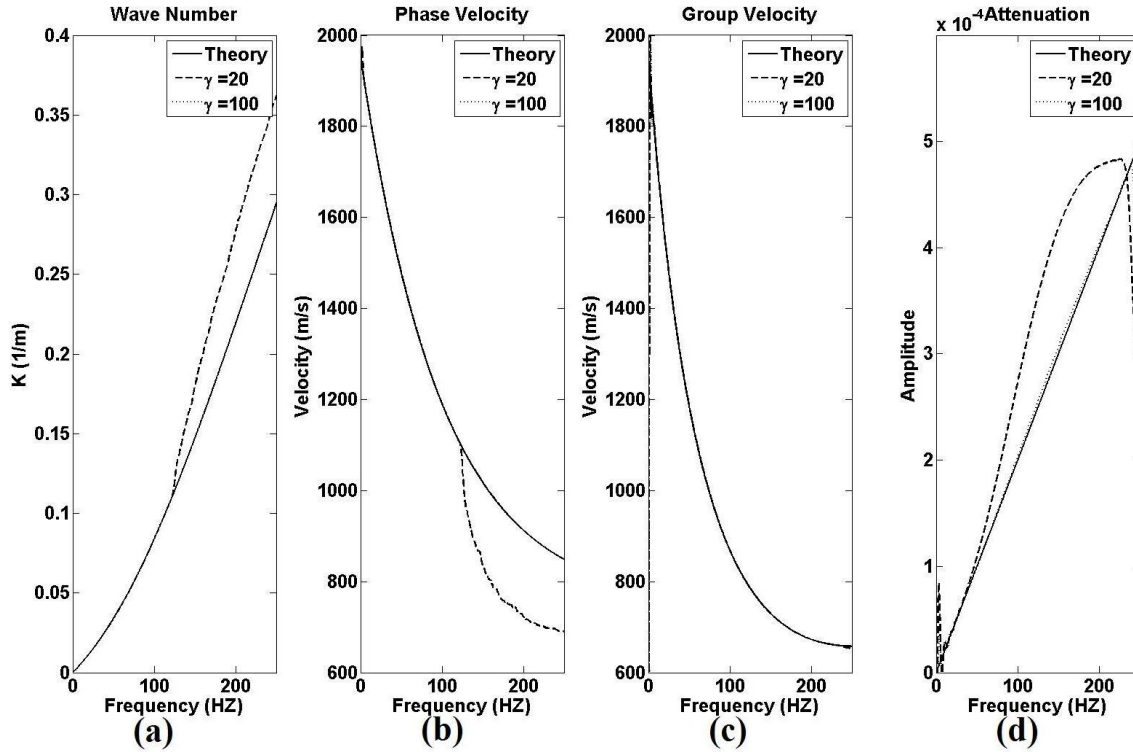
FIG. 5. The estimated propagation model parameters based on the scaling factors γ =20 and γ =100. (a) The wave number. (b) The phase velocity. (c) The group velocity. (d) The attenuation function.
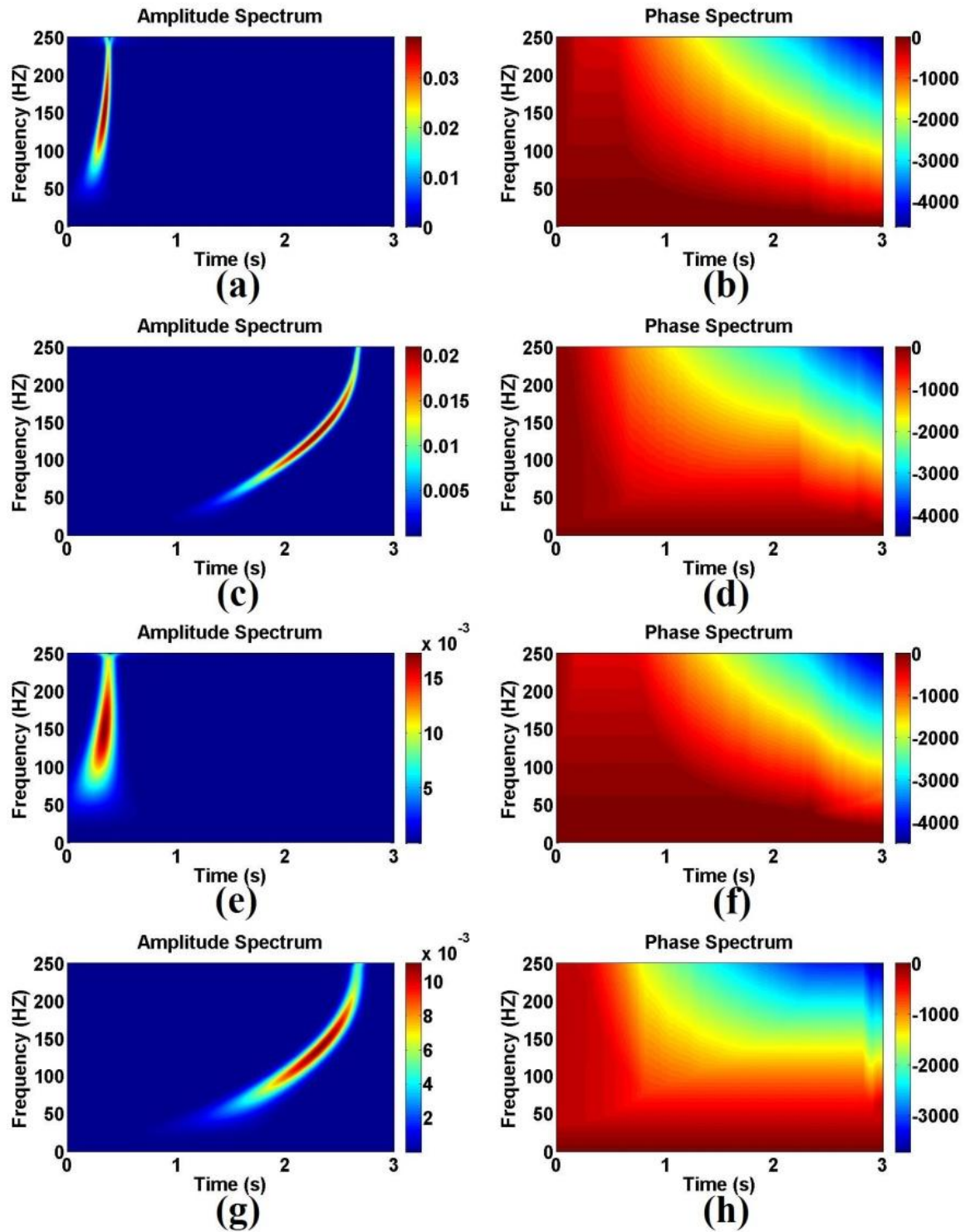
FIG 6. (a) and (c) the amplitude spectrum; (b) and (d) the phase spectrum for traces 1 and 7 respectively based on the scaling factor γ =20. (e) and (f) the amplitude spectrum; (g) and (h) the phase spectrum for traces 1 and 7 respectively based on the scaling factor γ =100.
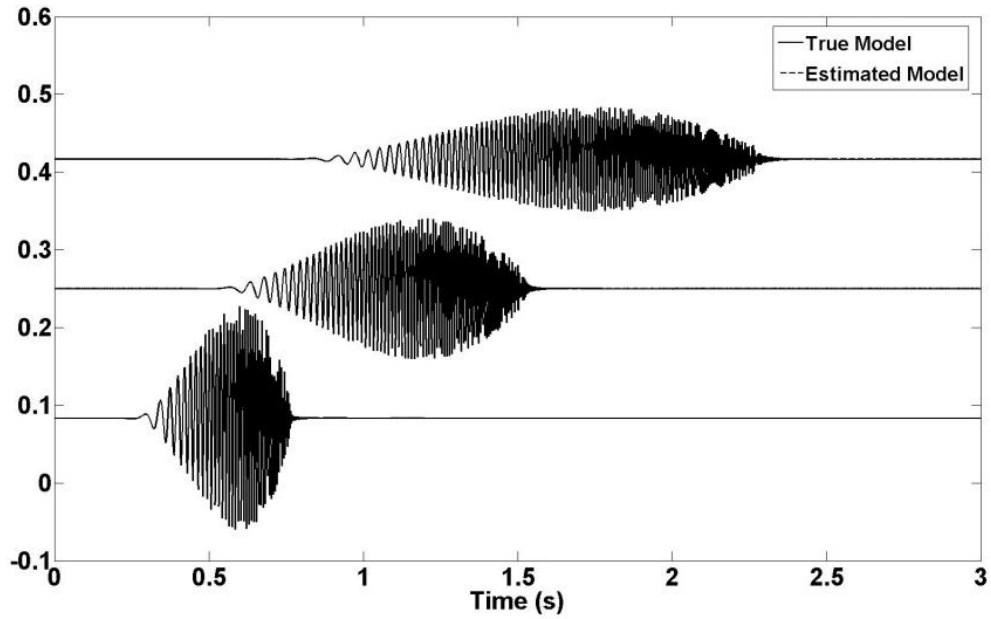
FIG. 7. The dashed lines are the predicted model for traces (2), (4) and (6) respectively.
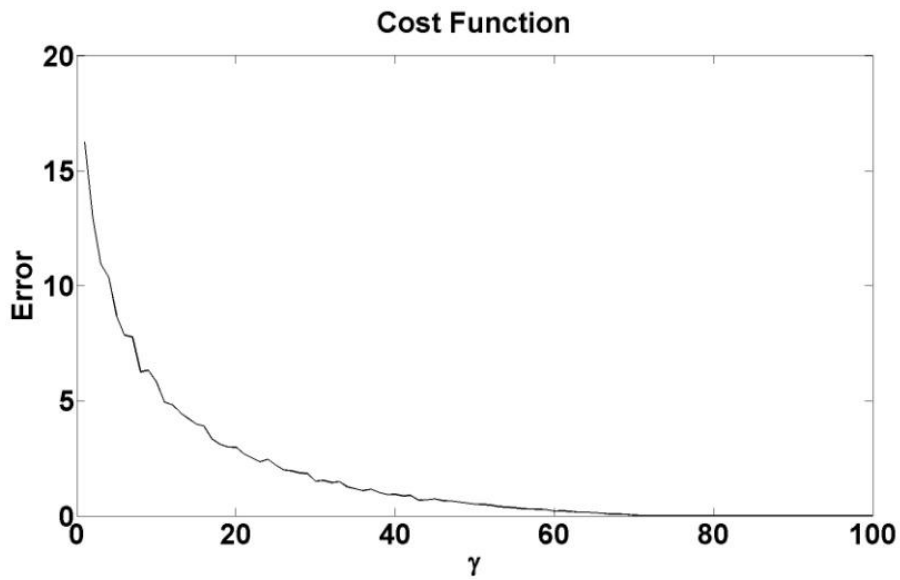
FIG. 8. The cost function for the data in Fig. 7.
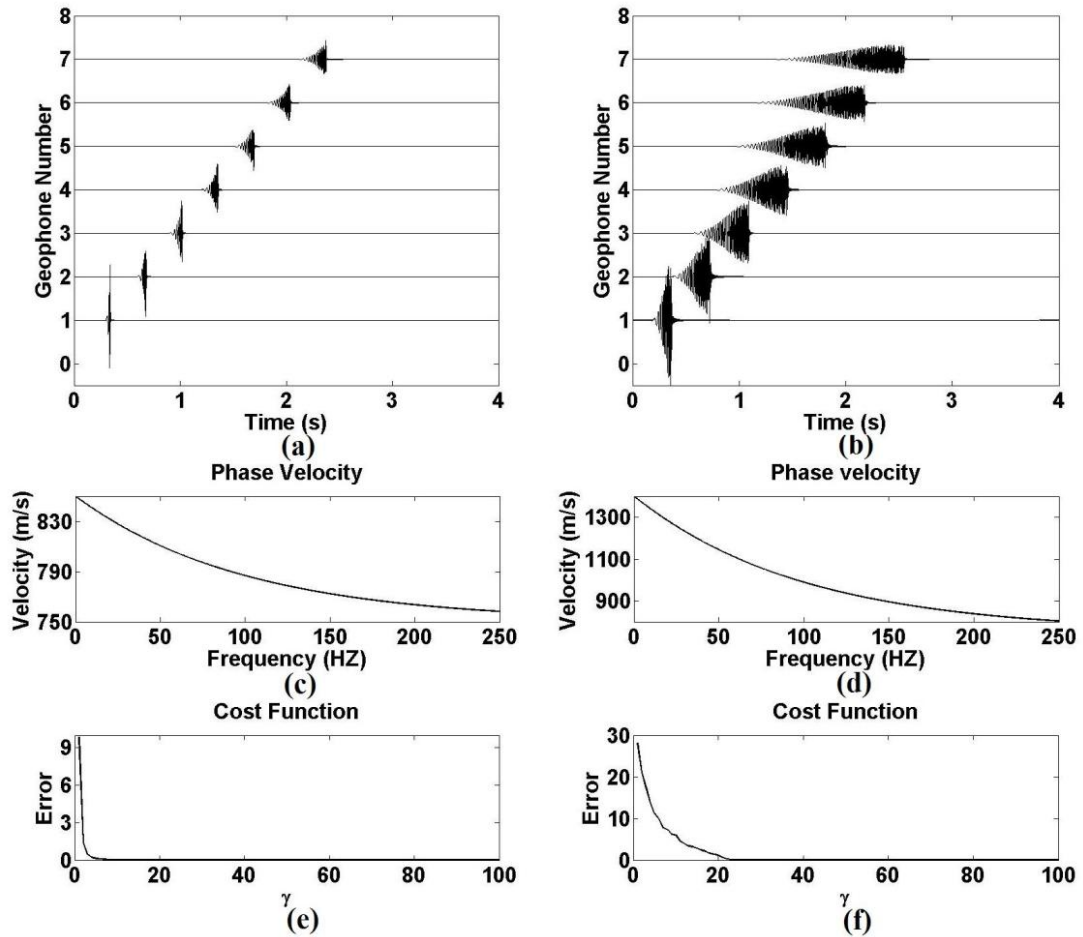
FIG. 9. (a) and (b) two different dispersed data sets. (c) and (d) the phase velocities for (a) and (b) respectively. (e) and (f) the cost functions for (a) and (b) respectively.
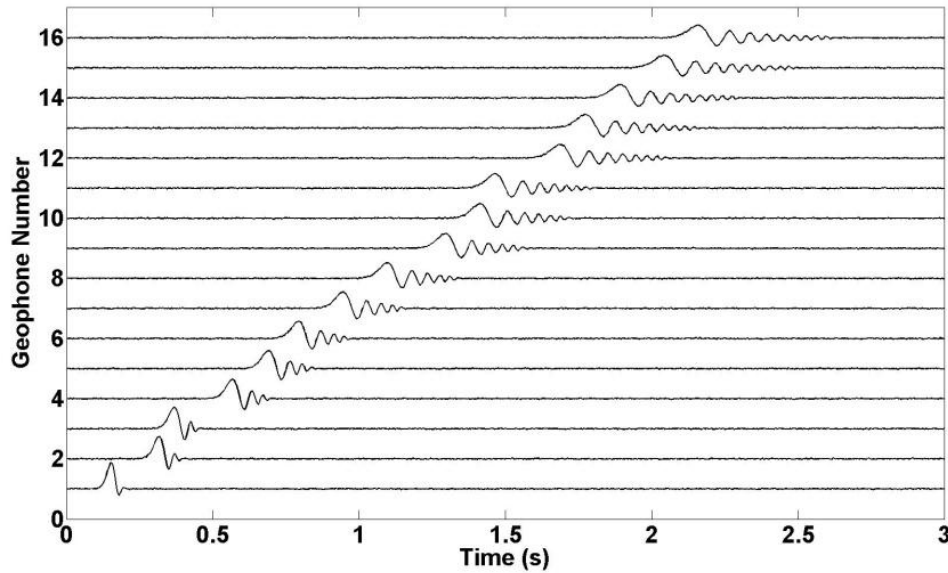
FIG. 10. A noisy synthetic seismic record with a dispersive Gaussian wavelet.
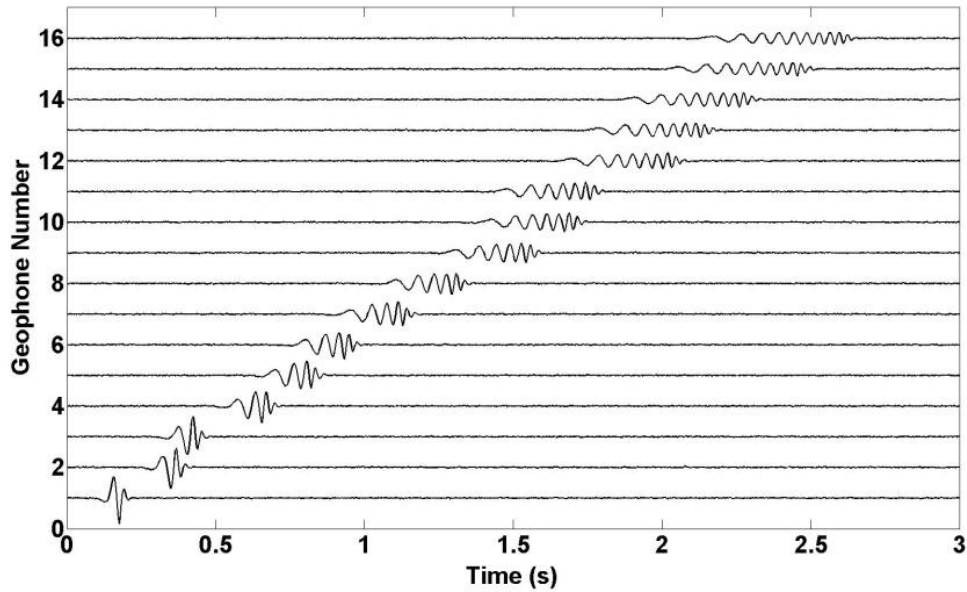
FIG. 11. A noisy synthetic seismic record with a dispersive Ricker wavelet.

(a) (b) (c) (d)
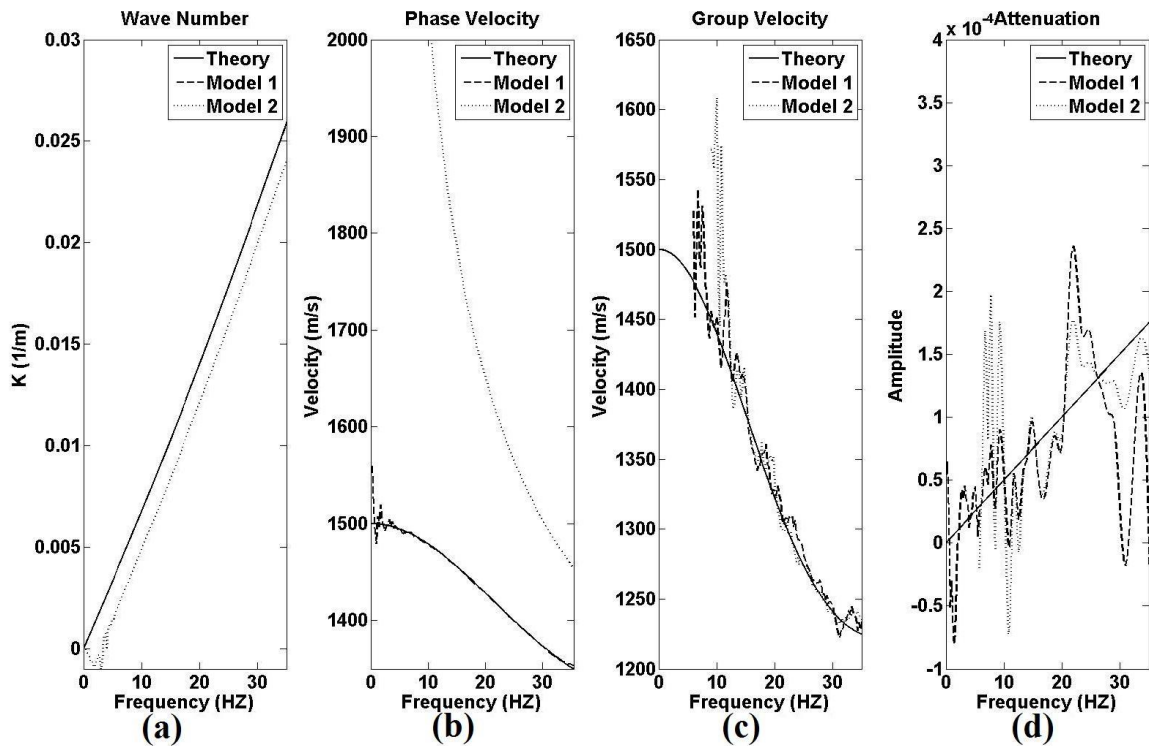
FIG. 12. The propagation model parameters. (a) The wave number. (b) The phase velocity. (c) The group velocity. (d) The attenuation function.
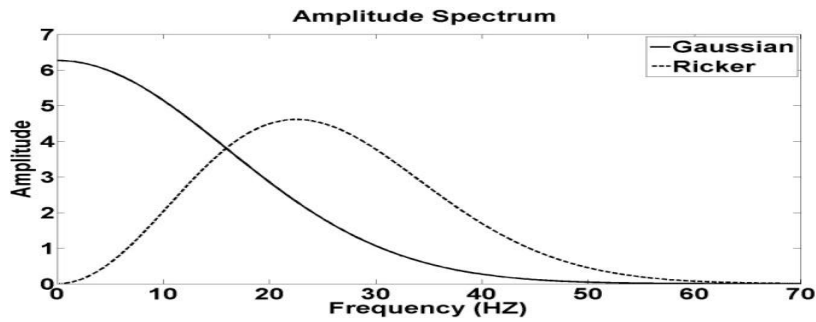
FIG. 13. The amplitude spectrum of the Gaussian wavelet (the solid line) and the Ricker wavelet (the dashed line).
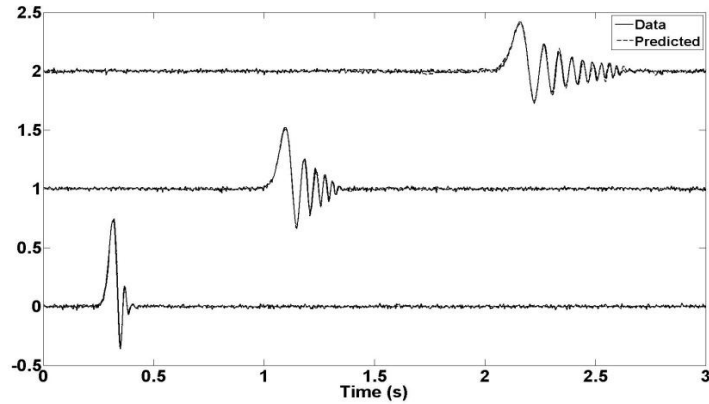
FIG. 14. The solid lines are traces for geophones (2), (9) and (15) of the first model and the dashed lines are the predicted traces based on the estimated wave number and attenuation function for geophones (2), (9) and (15) respectively.
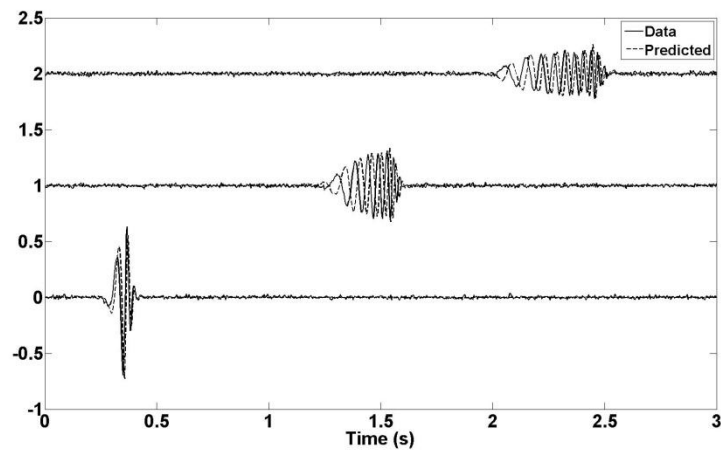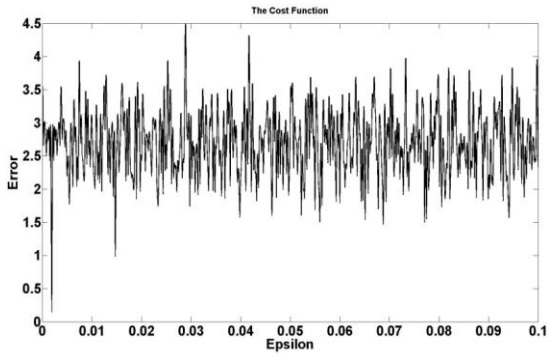

FIG. 15. The solid lines are traces for geophones (2), (9) and (15) of the second model and the dashed lines are the predicted traces based on the estimated wave number and attenuation function for geophones (2), (9) and (15) respectively.
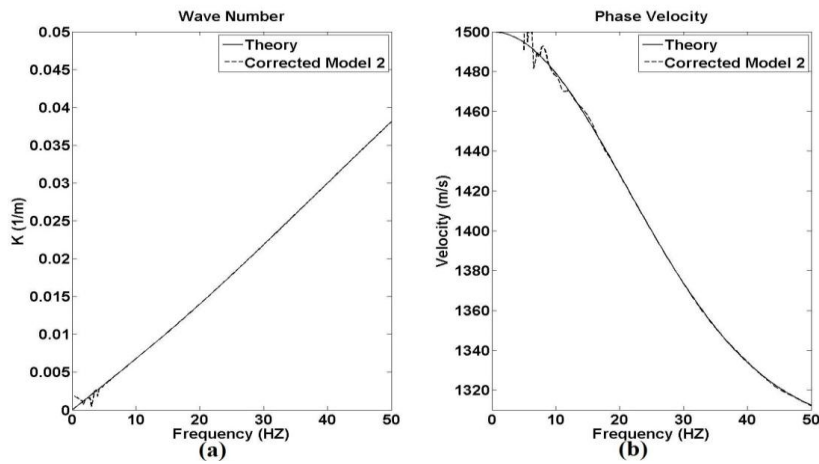
FIG. 16. The cost function for 0<ε<.1.

FIG. 17. (a) The wave number. (b) The phase velocity corrected based on computed optimum value for epsilon.
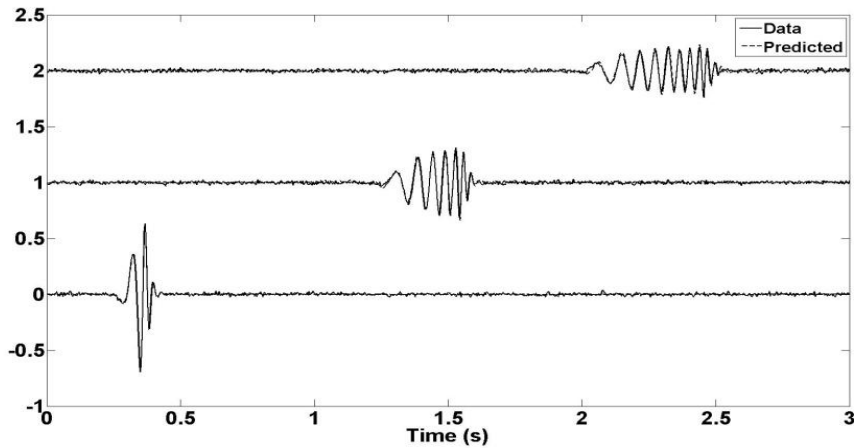

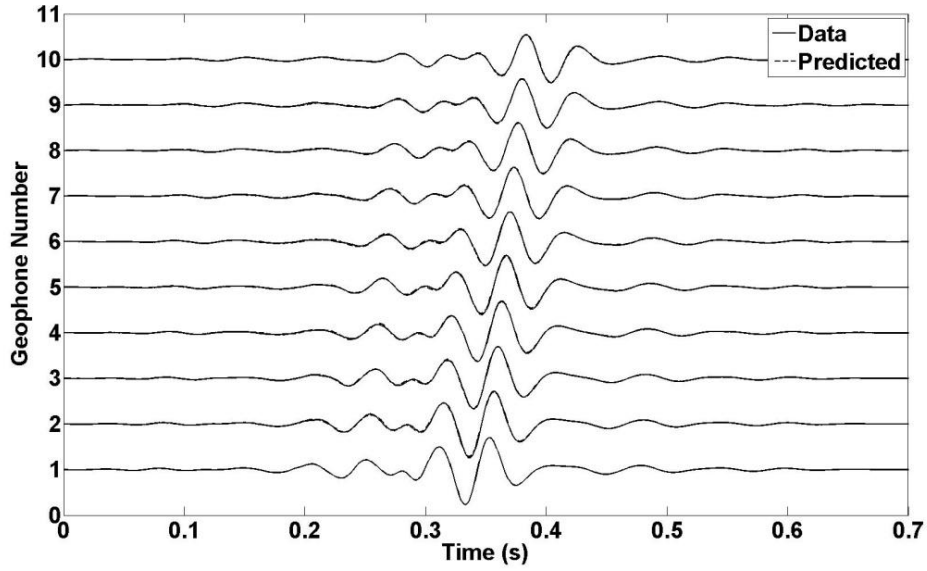FIG. 18. The predicted traces based on the corrected wave number.

FIG. 19. The real data (the solid lines) and the predicted (the dashed lines).
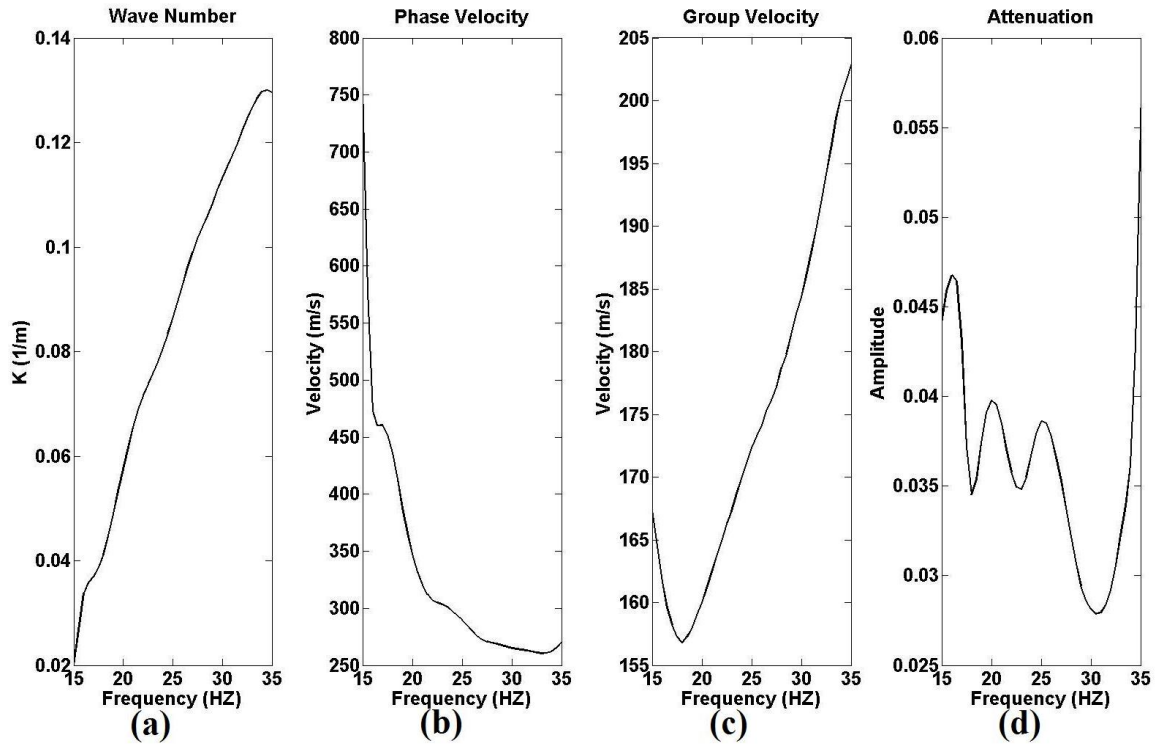

FIG. 20.   Estimated propagation model parameters of the real data. (a) The wave number. (b) The phase velocity. (c) The group velocity. (d) The attenuation function.